The 2009 IEEE/RSJ International Conference on
Intelligent Robots and Systems
October 11-15, 2009 St. Louis, USA

Modeling and Analysis of a Biomimetic Foot Mechanism

Jong-Tae Seo and Byung-Ju Yi, *Member, IEEE*

***Abstract*—Humans and mammals possess their own feet. Using the mobility of their feet, they are able to walk in various environments such as plain land, desert, swamp, and so on. Previously developed biped robots and four-legged robots did not employ such adaptable foot. In this work, a biomimetic foot mechanism is investigated through analysis of the foot structure of the human-being. This foot mechanism consists of a toe, an ankle, a heel, and springs replacing the foot muscles and tendons. Using five toes and springs, this foot can adapt to various environments. A mathematical modeling for this foot mechanism was performed and its characteristics were observed through numerical simulation.**

I. Introduction

RECENTLY developed locomotion mechanisms with feet can be classified as a bi-pedal robot and a four-legged robot. The well-known ASIMO [1] developed by Honda Co. Locomotion is the first successful humanoid robot. WABIAN-2 from Waseda University of Japan has a toe degree of freedom unlike ASIMO. This robot's walking is similar to the human walking because it has one toe [2]. H7 developed at the University of Tokyo uses various sensor informations in order to get a balance of robot [3]. Humans and animals have several toes. However, previous humanoid models have limitation in adaption to various environments because most of foot mechanisms are rectangular shaped. They can walk just on an even terrain. Though such foot mechanisms have a soft material like rubber [4] or spring [5] in order to absorb an impact from ground contact, they cannot structurally absorb the impact. Chung and Yi [6] analyzed the toe mechanisms of humans and animals. They claimed that multi-legged and multi-jointed foot structure was shown to be an intelligent mobility playing the role of impulse absorption and that prior to control action by actuators, passive adaptation to unknown environment is crucial.

In this work, we propose a biomimetic foot mechanism that can adapt to uneven terrain by utilizing the mobility of the foot structure. The effectiveness of the proposed foot mechanism is shown through simulation based on the dynamic model developed in this paper and a commercially available software.

This work was partially supported by the Korea Science and Engineering Foundation (KOSEF) grant funded by the Korea government (R01-2008-000-11742-0), partially supported by the GRRC program of Gyeonggi province (2008-041-0003-0001), partially supported by the research fund of HYU (HYU-2008-T), partially supported by the Ministry of Knowledge Economy (MKE) and Korea Industrial Technology Foundation (KOTEF) through the Human Resource Training Project for Strategic Technology, and the outcome of a Manpower Development Program for Energy & Resources supported by the Ministry of Knowledge and Economy (MKE).

J.-T. Seo and B.-J. Yi are with the school of electrical engineering and computer science, Hanyang University, Ansan, Korea (corresponding author to provide phone: +82-31-400-5218; fax: +82-31-416-6416; e-mail: bj@hanyang.ac.kr).

II. The Human Foot

Fig. 1 shows the skeleton and muscle of the human foot. The human foot consists of a hind foot, a mid-foot, and a forefoot. The human foot is composed of 52 bones, 60 joints, 214 tendons, 38 muscles, and a lot of blood vessels. These blood vessels connect the foot to the spinal cord, heart, and brain. The top of the foot plays the role of absorbing an impact in walking and supporting weight through strong connection to the foot's bones.

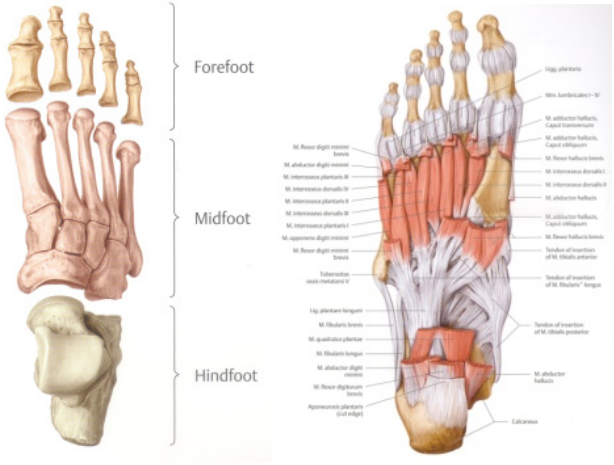

(a) (b)

Fig. 1. (a) The bone of the foot from the dorsal view, Right: the intrinsic foot muscles from the plantar view [7].

A. The Longitudinal Arch of the Foot

The main passive stabilizers of the longitudinal arch are the plantar aponeurosis, the Lig.plantare longum, and the Lig.calcaneonaviculare plantare. The plantar aponeurosis is particularly important owing to its long lever arm, while the Lig.calcaneonaviculare plantare is the weakest component. The M.flexor hallucis longus, which runs beneath the Sustentaculum tali, is particularly effective in tightening the longitudinal arch like the chord of an arc [7]. Ren et al. [8] proposed that foot's functions are highly dependent on gait phase, which is a major characteristic of human locomotion. In this paper, similar to the arch foot as shown in Fig. 2, we propose a 4-bar linkage of Fig. 3 as the foot model. This mechanism uses a spring between bones in order to obtain shock-absorbing effect at the arch [9].

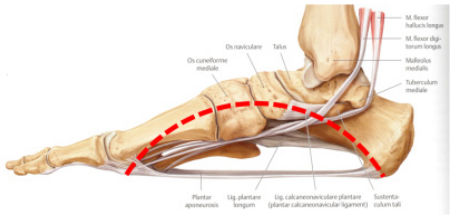

Fig. 2. Support of the longitudinal arch [7].

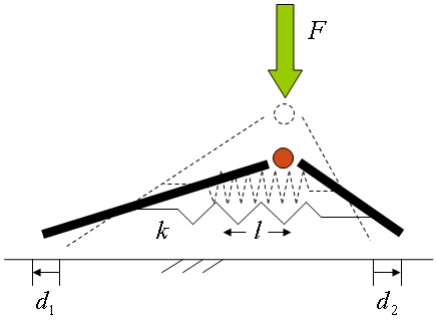

Fig. 3. The 4-bar linkage with an arch similar to the human foot.

B. The Movements of the Foot

Fig. 4(a) shows the motion of the subtalar joint. Rotation of the calcaneus medially (inversion) and laterally (eversion) is measured from the neutral (zero-degree) position. This is done clinically by holding the leg stationary and moving the calcaneus back and forth. Estimation of the range of inversion/eversion is based on the calcaneal axis. Fig. 4(b) shows the motion that is tested with the hindfoot fixed. Pronation/supination of the forefoot is tested by rotating the forefoot outward relative to the hindfoot (raising the lateral border of the foot), or inward (raising the medial border of the foot). Fig. 4(c) shows the motion of the joints of the big toe. The toes and especially the big toe can be passively extended to approximately 90°. This is an important prerequisite for walking, especially during the phase between the heel take-off and the toe strike [9].

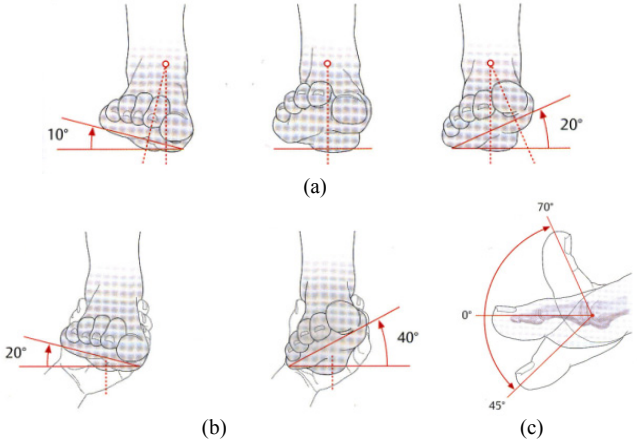

Fig. 4. Range of motion of the joints of the foot [7].

C. Stance Phase

The stance phase begins when the heel contacts the ground (heel strike) and ends when the toes push off from the ground (toe off). This phase makes up 60% of the gait cycle. The swing phase begins with the toe-off and ends with the heel strike. It makes up 40% of the gait cycle. (100% of gait cycle = the period between two heel strikes of the same foot)[10]

D. Foot Design

Fig. 5 shows a biomimetic foot mechanism, which reflects the structure and movement of the human foot. This foot mechanism consists of 5-toes, 5-metatarsus, an ankle, a heel, and 15-springs replacing the foot muscles and tendons. And the rotational motion of mid-foot can be created by combination of 5-chains. Also the toes can be moved up and down.

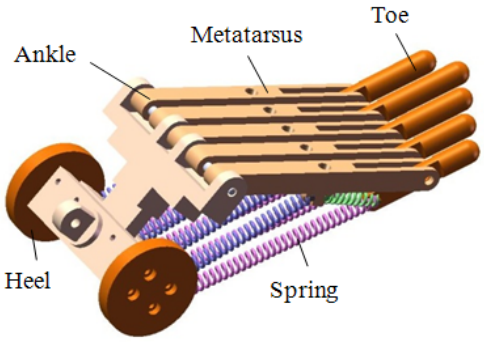

Fig. 5. Biomimetic foot mechanism.

III. Stiffness Modeling

Fig. 6 represents a planar 3 DOF biomimetic foot model. There exists a bi-articular-type spring k_{d3} as well as mono articular-type springs k_{d1}, k_{d2}. Fig. 7 shows the kinematic parameters of the 3-DOF biomimetic foot model. Fig. 8 represents the geometry of each spring and kinematic parameters of the 3-DOF biomimetic foot model.

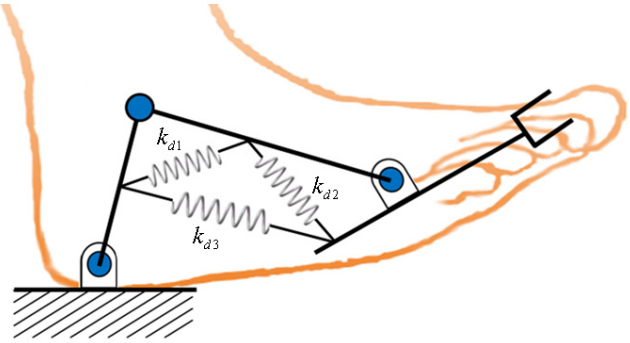

Fig. 6. 3-DOF Biomimetic foot model.

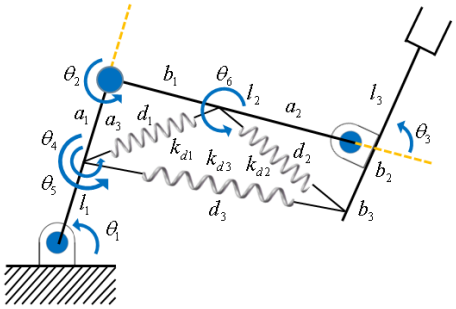

Fig. 7. Kinematic parameters of a biomimetic foot model.

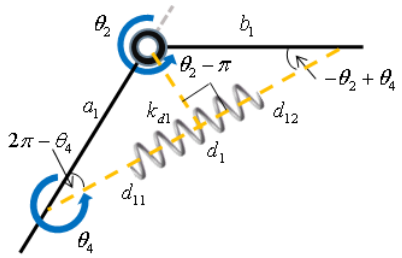

(a) Geometric model for sping d_1

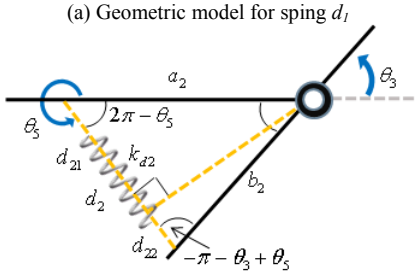

(b) Geometric model for sping d_2

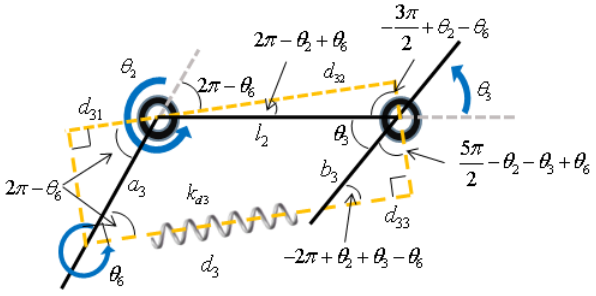

(c) Geometric model for sping d_3

Fig. 8. Geometry of springs and kinematic parameters of a biomimetic foot model.

The relationship between the stiffness matrix $\left[K_{\phi\phi}\right]\in R^{2\times2}$ in the joint space and the stiffness matrix $\left[K_{dd}\right]\in R^{3\times3}$ in the spring space is defined as [11]

$$\left[K_{\phi\phi}\right]=\left[G_{\phi}^{d}\right]^{T}\left[K_{dd}\right]\left[G_{\phi}^{d}\right], \tag{1}$$

where the stiffness matrices in the spring space and the joint space are defined, respectively, as

$$\left[K_{dd}\right]=\begin{bmatrix}k_{d3}&0&0\\0&k_{d1}&0\\0&0&k_{d2}\end{bmatrix}$$
$$\left[K_{\phi\phi}\right]=\begin{bmatrix}k_{11}&k_{12}\\k_{21}&k_{22}\end{bmatrix}, \tag{2}$$

and Jacobian $\left[G_{\phi}^{d}\right]\in R^{2\times2}$ relating the two independent joint (θ_2, θ_3) variables (i.e., the two joints in the serial chain) to the three spring displacements (d_1, d_2 and d_3) is given as

$$\left[G_{\phi}^{d}\right]=\begin{bmatrix}g_2^{d_3}&g_3^{d_3}\\g_2^{d_1}&0\\0&g_3^{d_2}\end{bmatrix},\qquad \left(g_j^{d_i}=\frac{\partial d_i}{\partial\phi_j}\right) \tag{3}$$

where from the geometric model of Fig. 8, the components of the Jacobian $\left[G_{\phi}^{d}\right]$ can be expressed as

$$\begin{aligned}g_1^{d_3}&=-l_2\sin(\theta_2-\theta_6)+b_3\sin(\theta_2+\theta_3-\theta_6)\\g_2^{d_3}&=b_3\sin(\theta_2+\theta_3-\theta_6)\\g_1^{d_1}&=-b_1\sin(\theta_2-\theta_4)\\g_2^{d_2}&=b_2\sin(\theta_3-\theta_5).\end{aligned} \tag{4}$$

From (1), the relationship between stiffness components is found as

$$\begin{bmatrix}k_{11}\\k_{12}\\k_{22}\end{bmatrix}=\begin{bmatrix}\left(g_2^{d_3}\right)^2&\left(g_2^{d_1}\right)^2&0\\g_2^{d_3}g_3^{d_3}&0&0\\\left(g_3^{d_3}\right)^2&0&\left(g_3^{d_2}\right)^2\end{bmatrix}\begin{bmatrix}k_{d3}\\k_{d1}\\k_{d2}\end{bmatrix}. \tag{5}$$

IV. Dynamic Modeling

In this section, we derive the dynamic model for the foot mechanism of Fig. 5, which is composed of five parallel closed-chains. Fig. 9 denotes one closed-kinematic loop of the proposed foot mechanism. If the link length l_2 is not zero, it can be analyzed as a 5-bar and if l_2 is zero, it can be analyzed as a 4-bar. In this section, we analyze this loop as a 5-bar. Since mobility of this model is 2, the independent joints (θ_1, θ_2) are set as ϕ_a, the dependent joints (θ_3, θ_4, θ_5, d_1, and d_2) as ϕ_p, and the joints (θ_1, θ_2, θ_3, θ_4) of the serial open-chain are set as ϕ.

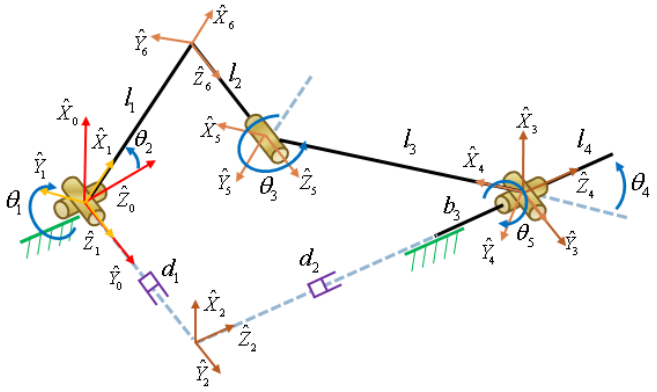

Fig. 9. One closed-chain model for the dynamic analysis.

Using the virtual work principle, the dynamics of the open chain is obtained by cutting the joint θ_5 that contacts the open-chain to the ground can be directly incorporated into the closed chain dynamics according to

$$\delta W=\tau_a^T\delta\phi_a=\tau_\phi^T\delta\phi, \tag{6}$$

where τ_a is the independent joint torque of the 5-bar linkage and τ_ϕ is the joint torque of the 4 DOF serial open-chain. And the relationship between ϕ and ϕ_a is obtained as

$$\delta\phi = \left[G_a^{\phi} \right] \delta\phi_a . \tag{7}$$

Substituting (7) into (6), the motion torque (inverse dynamic) model can be expressed in terms of the independent joint set as

$$\begin{aligned} \tau_a &= \left[G_a^{\phi} \right]^T \tau_{\phi} \\ &= \left[I_{aa}^* \right] \ddot{\phi}_a + \dot{\phi}_a^T \left[P_{aaa}^* \right] \dot{\phi}_a , \end{aligned} \tag{8}$$

where $\left[I_{aa}^* \right]$ and $\left[P_{aaa}^* \right]$ denote the inertial matrix and inertia power array defined in the independent joint set, respectively [12].

Congregating the motion torque of the five chains, we have

$$\begin{aligned} \tau_{motion} &= \sum_{r=1}^{5} \left(\left[{}_r I_{aa}^* \right] \ddot{\phi}_a + \dot{\phi}_a^T \left[{}_r P_{aaa}^* \right] \dot{\phi}_a \right) \\ &= \left(\sum_{r=1}^{5} \left[{}_r I_{aa}^* \right] \right) \ddot{\phi}_a + \dot{\phi}_a^T \left(\sum_{r=1}^{5} \left[{}_r P_{aaa}^* \right] \right) \dot{\phi}_a . \end{aligned} \tag{9}$$

The motion torque (τ_{motion}) of the foot can be created by external torque ($\tau_{external}$) due to weight, spring force, and damping force. Thus, the dynamic equation of the foot is denoted as

$$\tau_{external} = \tau_{stiffness} + \tau_{damper} + \tau_{weight} \tag{10}$$

where $\tau_{stiffness}$, τ_{damper} , and τ_{weight} denote the external torque by stiffness, damper, and weight, respectively. The external torque with regard to the independent joint stiffness can be expressed as

$$\tau_{stiffness} = \sum_{r=1}^{5} \left[{}_r k_{aa} \right] \delta\phi_a , \tag{11}$$

where $\left[{}_r k_{aa} \right]$ of the *r-th* closed-chain can be expressed in terms of the muscle joint set as

$$\begin{aligned} \left[{}_r k_{aa} \right] &= \left[{}_r G_a^{\phi} \right]^T \left[{}_r K_{\phi\phi} \right] \left[{}_r G_a^{\phi} \right] \\ &= \left[{}_r G_a^{\phi} \right]^T \left(\left[{}_r G_{\phi}^{d} \right]^T \left[{}_r K_{dd} \right] \left[{}_r G_{\phi}^{d} \right] \right) \left[{}_r G_a^{\phi} \right], \end{aligned} \tag{12}$$

where $\left[{}_r G_a^{\phi} \right]$ denotes the Jacobian relating the coordinates of the *r-th* open chain to the independent coordinates, and $\left[{}_r K_{\phi\phi} \right]$ is defined in (1).

The external torque in terms of the joint damper can be expressed as

$$\tau_{damper} = \sum_{r=1}^{5} \left[{}_r b_{aa} \right] \dot{\phi}_a , \tag{13}$$

where $\left[{}_r b_{aa} \right]$ of the *r-th* closed-chain can be expressed as

$$\begin{aligned} \left[{}_r b_{aa} \right] &= {}_r \left[G_a^{\phi} \right]^T \left[{}_r B_{\phi\phi} \right] \left[{}_r G_a^{\phi} \right] \\ &= \left[{}_r G_a^{\phi} \right]^T \left(\left[{}_r G_{\phi}^{d} \right]^T \left[{}_r B_{dd} \right] \left[{}_r G_{\phi}^{d} \right] \right) \left[{}_r G_a^{\phi} \right]. \end{aligned} \tag{14}$$

The external torque by weight can be expressed as

$$\left[\tau_{weight}^* \right] = \sum_{r=1}^{5} \left\{ \left[{}_r G_a^{\phi} \right]^T \left(\left[{}_r G_{\phi}^{c} \right]^T \begin{bmatrix} -mg \\ 0 \\ 0 \end{bmatrix} \right) \right\} \tag{15}$$

where $\left[G_{\phi}^{c} \right]$, m, and g denote the Jacobian at the mass center of each link, mass, and gravitational constant, respectively. By rearranging (9) with respect to the angular acceleration, we have

$$\ddot{\phi}_a = \left(\sum_{r=1}^{5} \left[{}_r I_{aa}^* \right] \right)^{-1} \left\{ -\dot{\phi}_a^T \left(\sum_{r=1}^{5} \left[{}_r P_{aaa}^* \right] \right) \dot{\phi}_a + \tau_{external} \right\} \tag{16}$$

where $\tau_{external}$ is from (10).

Integrating (16) with respect to time twice yields the joint angles at the independent joints. The dynamic model driven in this section is used to simulate the foot mechanism and optimize its structure.

V. Simulations

A. Simulation based on dynamic model

This section shows simulation results for the stiffness and dynamic models of the proposed foot mechanism. Fig. 10 shows a dynamic simulator of the biomimetic foot mechanism based on the dynamic model derived in section VI. Table 1 shows the kinematic and dynamic parameters for the single chain. The weight applied to one foot is set as one half of that of a human-body with 52 kg. The kinematic and dynamic parameters of the other chains are identical. Friction in the ground is ignored. k_{di} and b_{di} denote the stiffness and the damping constant in the spring space, respectively. Those parameters were selected based on the human foot data [7, 9]. Fig. 11 shows the foot motion when a weight of 26 kg is applied vertically at the ankle position. Using the dynamic model of (16), Fig. 12 shows the simulation result of the foot tilted by 10° when the weight is applied at the same position.

TABLE I
KINEMATIC PARAMETERS FOR THE SINGLE CHAIN

Parameter	Value
Link lengths	l_1=0.02 m, l_2=0.02 m, l_3=0.04 m, l_4=0.015 m
Stiffness	k_{d1}=k_{d2}=k_{d3}=12,000 N/m
Damping coefficient	b_{d1}=b_{d2}=b_{d3}=200 Ns/m
Weight	26 kg

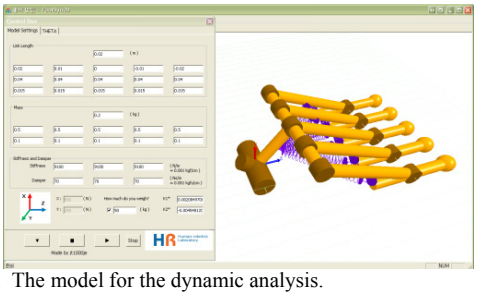

Fig. 10. The model for the dynamic analysis.

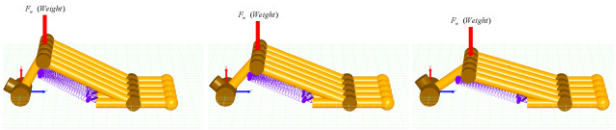

Fig. 11. The foot motion when the weight is applied.

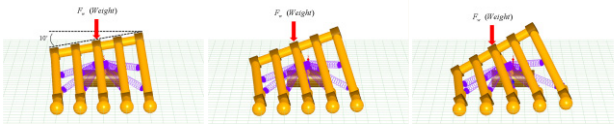

Fig. 12. Motion of the foot tilted by 10° when the weight is applied to the vertical direction.

B. *Simulation based on commercial software*

In order to corroborate the simulation result conducted in the previous section, we perform simulation for the foot behavior in the virtual environment using a commercially available dynamic simulation program named DAFUL, which is developed by Virtual Motion, Inc. [13]. Fig. 13 and Fig. 14 show that the simulation results are almost identical to Fig. 11 and Fig. 12. The motion of the biomimetic foot can be simulated not only for the flat surface, but also for uneven surface. Fig. 15 shows that the biomimetic foot can adapt to an uneven surface in a safe manner.

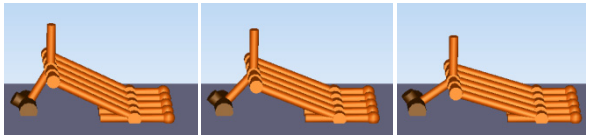

Fig. 13. The foot motion when a weight is applied (DAFUL).

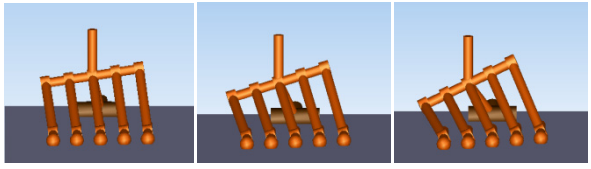

Fig. 14. Motion of the foot tilted by 10° when a weight is applied to the vertical direction (DAFUL).

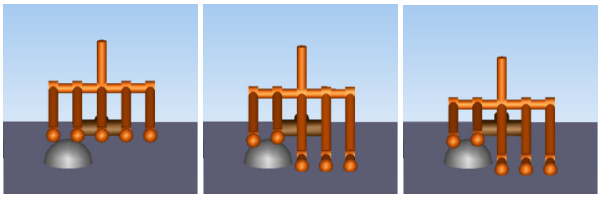

Fig. 15. Motion at uneven surface (DAFUL).

C. *Simulation in the virtual environment*

For the biomimetic foot, a more complex simulation is conducted. Fig. 16(a) shows a virtual environment and a walking machine equipped with the foot mechanism. The side motion of the mechanism is constrained, and only the up-and-down motion is allowed. Thus, the walking motion can be controlled by one actuator. The trajectory of the foot is given by a similar motion pattern [3] of the human foot. The muscle of the sole of the foot is modeled by a virtual spring. An Achilles' tendon in the human leg is modeled by a suspension. The virtual environment consists of a plat surface and a partially rough surface. Fig. 16(b) and Fig. 16(c) show that the foot of the robot is able to walk and overcome the uneven surface by wrapping or grasping the terrain by the multi-jointed foot mechanism.

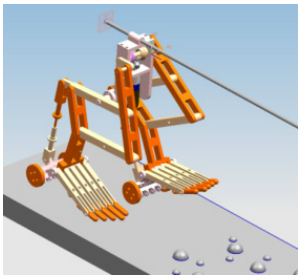

(a) Simulation model

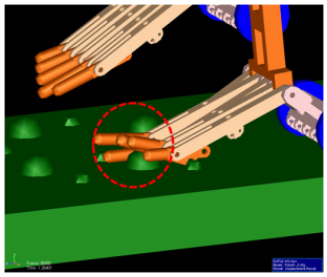

(b) Toe motion at the rough surface

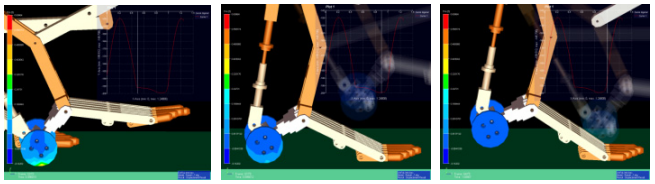

(c) Stance phase

Fig. 16. Walking simulations (DAFUL).

D. *Landing Simulation*

The biomimetic foot is also effective in the landing motion. Fig. 17 shows the landing simulation for a flat foot and a bio-mimetic foot at the even terrain. The robot configuration at the initial contact state is set such that ZMP is within the footprint. Fig. 18 shows the landing simulation for a flat foot and a bio-mimetic foot at a simply uneven terrain. Fig. 19 shows the landing simulation for a flat foot and a bio-mimetic foot at a complex uneven terrain. For the latter cases, both feet land on the ground in a safe manner. It is noted that the biomimetic foot is very effective in the landing motion even in uneven terrains, while the flat foot is not successful in landing in such terrains. In these simulations, no control is involved. The motion is just based on the system dynamics. Therefore, it is believed that the biomimetic foot model proposed in this work is feasible as a robot foot mechanism, which can be possibly incorporated into a foot of a biped robot or a multi-legged robot.

Video clips attached to this paper clearly demonstrate the behavior of the biomimetic foot.

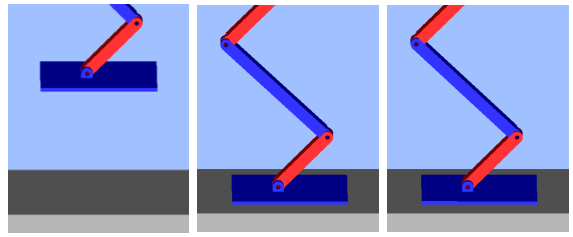

(a) Flat foot

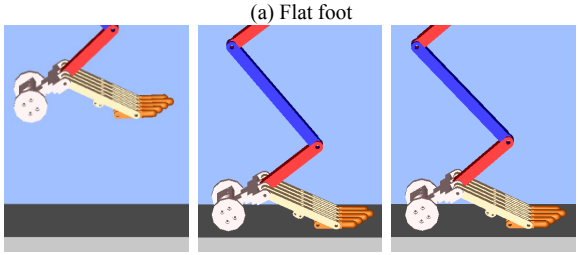

(b) Bio-mimetic foot

Fig. 17. Landing simulation at the even terrain.

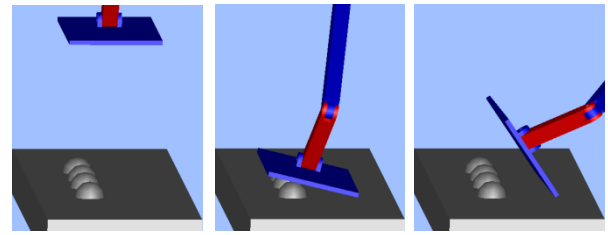

(a) Flat foot

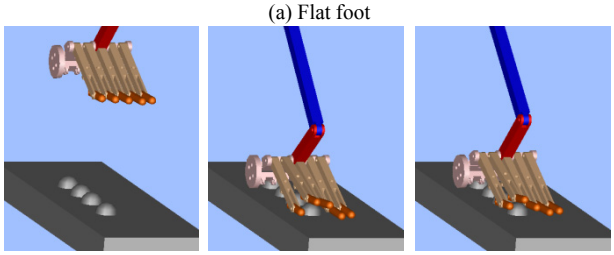

(b) Bio-mimetic foot

Fig. 18. Landing simulation at the simply uneven terrain (DAFUL).

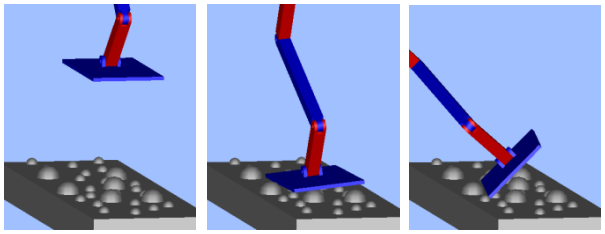

(a) Flat foot

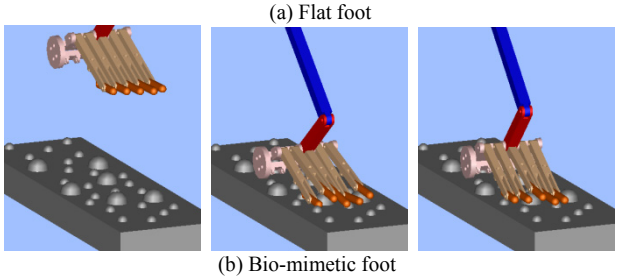

(b) Bio-mimetic foot

Fig. 19. Landing simulation at the complex uneven terrain (DAFUL).

E. Passive Anatomy

The inherent intelligent structures (multi-chains, multi -joints, and multiple contacts) of the general biomechanical systems passively adapt to environments prior to the control action by actuators [6]. As a result, it distributes and reduces impulse, and also improves stability as discussed in this paper. It would also alleviate the burden in the post control action after the passive adaptation.

VI. Conclusions

The contribution of this paper is to propose a biomimetic foot mechanism that is similar to the human foot. Firstly, kinematic, stiffness, and dynamic model for this foot mechanism are derived. Secondly, we show the behavior of the proposed foot mechanism through a virtual simulation based on dynamic model of this mechanism along with comparion to a commercial software. We also verified the effectiveness of the foot mechanism through simulation for walking and landing behaviours. It is believed that the mobility of the proposed foot structure will play a vital role of stable walking even in the presence of uneven terrain. Future work is implementation of the biomimetic foot mechanism to a real biped robot or a multi-legged robot.

References

[1] Y. Sakagami, R. Watanabe, C. Aoyama, S. Matsunaga, N. Higaki and K. Fujimura, "The intelligent ASIMO: system overview and integration," in *Proc. IEEE/RSJ Int. Conf. Intell. Robots and Systems*, 2003, pp. 2478-2483.

[2] Y. Ogura, K. Shimomura, H. Kondo et. al., "Human-like walking with knee stretched, heel-contact and toe-off motion by a humanoid robot," in *Proc. IEEE/RSJ Int. Conf. Intell. Robots and Systems*, 2006, pp. 3976-3981.

[3] Y. Takahashi, K. Nishiwaki, S. Kagami, H. Mizoguchi, H. Inoue, "High-speed pressure sensor grid for humanoid robot foot," in *Proc. IEEE/RSJ Int. Conf. Intell. Robots and Systems*, 2005.

[4] J. Li, Q. Huang, W. Zhang, Z. Yu, and K. Li, "Flexible foot design for a humanoid robot," in. *Proc IEEE Int. Conf. Automation and Logistics*, 2008, pp.1414-1419.

[5] H. Yang, M. Shuai, Z. Qiu, H. Wei, Q. Zheng, "A novel design of flexible foot system for humanoid robot," in Proc IEEE Conf. Robotics, Automation and Mechtronics, 2008, pp.824-828.

[6] J.H. Chung and B.-J. Yi, "Intelligent mobility playing the role of impulse absorption," in *Proc. Int. Conf. Distributed Autonomous Robotic Systems*, 2008.

[7] M. Schuenke, E. Schulte, U. Schumacher, et. al., *General Anatomy and Musculoskeletal System*. Thieme, 2006.

[8] L. Ren, D. Howard, L.-Q. Ren, C. Nester, L.-M. Tian, "A Phase-dependent hypothesis for locomotor functions of human foot complex," *Journal of Bionic Engineering*, vol. 5, pp. 175–180, 2008.

[9] M. Davis, Foot Design for a Humanoid Robot. The University of Queensland, 2004.

[10] C.L. Vaughan, B.L. Davies, J.C. O'Connor, Dynamics of Human Gait, *Kiboho Publisher* 1999.

[11] W. K. Kim, B.-J. Yi, and W. Cho, "RCC characteristics of planner/spherical three degree-of-freedom parallel mechanisms with joint compliances," *ASME Trans. J. Mechanical Design*, vol. 122, pp. 10-16, 2000.

[12] J. H. Lee, B.-J. Yi, I. H. Suh, "Biomimetic trajectory planning via redundant actuation," in: *Proc IEEE/RSJ Int. Conf. Intell. Robots and Systems*, 2000, pp. 1778-1784.

[13] DAFUL simulator : http://www.virtualmotion.co.kr/eng/